PC3246 Astrophysics I Project Report

Reproducing and analysing Stefansson et al. 2023's paper, "A Neptune-mass exoplanet in close orbit around a very loss-mass star challenges formation models"

Kushagra Shrivastava (A0281477U)[1]

[1]Department of Physics, National University of Singapore, Singapore

Semester 2, Academic Year 24/25

Contents

1 Introduction

Exoplanet detection is a challenging feat, especially for exoplanets orbiting lower luminosity stars such as M-type dwarfs. Stefánsson et al., 2023 discovers a high mass exoplanet, LHS3154b, in a short period orbit around a M-type dwarf using the Radial Velocity method, which is unexplained using current planetary formation model. Their Radial Velocity estimation from the obtained spectra are also based on a template-matching algorithm and not on theoretical spectra. In this paper, we explore the astrophysical background behind the exoplanet discovery and planet formation, and try to replicate the values obtained by Stefánsson et al., 2023 in their Table 1. We only aim to replicate the Planetary parameters, and not all the star parameters estimated by Stefánsson et al., 2023 through different scaling relations.

M-dwarfs are the coolest and the least massive Main Sequence stars with Morgan-Keenan luminosity class of V. Due to their low masses, the rate of hydrogen fusion is so slow which makes them stay on the main sequence for a extremely long period. Therefore, they are one of the most abundant type Main Sequence stars in our galaxy. Given their abundance, they are a target for exoplanet detection.

The M-dwarf in this work is LHS3154 discovered using parallax measurements by the Gaia telescope (Gaia Collaboration et al., 2023). It has a Right Ascension (α) of $16^{\mathrm{h}}\ 06^{\mathrm{m}}\ 32.78^{\mathrm{s}}$ and Declination (δ) of $+40°\ 54'\ 24.64''$. It is located in the constellation of Hercules, as shown in Figure 1 .

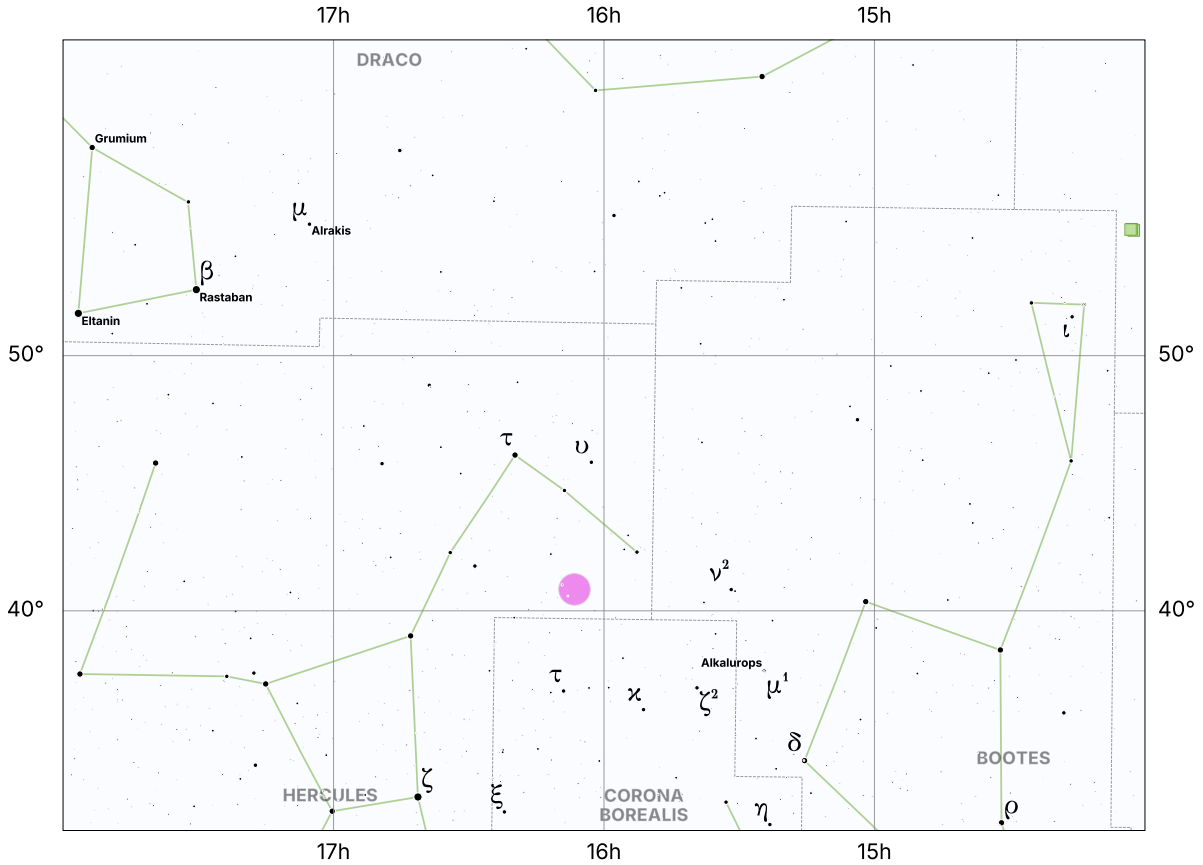

Figure 1: Position of LHS3154 shown by the pink circle in the constellation of Hercules with $\alpha = 16^{\mathrm{h}}\ 06^{\mathrm{m}}\ 32.78^{\mathrm{s}}$ and $\delta = +40°\ 54'\ 24.64''$. The star chart is created using `Starplot` library.

2 Data Acquisition and Methodology

2.1 Stellar Spectra Measurement and Radial Velocity calculation

The spectra measurements were taken using the Habitable-zone Planet Finder (HPF), a near-infrared spectrograph with resolving power of $R = 55,000$ on the 10-m Hobby-Eberly Telescope at USA's McDonald Observatory in Texas, USA. Further details about spectra collection are mentioned in Stefánsson et al., 2023 Supplemenatry Text. All the raw spectra are available at https://github.com/gummiks/hpfserval_lhs3154 and were used to reproduce the results.

137 spectra were gathered in 69 visits, and as mentioned by Stefánsson et al., 2023, we removed all the spectra with a Signal to Noise ratio less than 15. The Earth's sky background spectra and the Telluric lines were erased from these spectra. Telluric lines are caused by molecules such as oxygen, water, and ozone in the Earth's atmosphere. Furthermore, the spectra obtained on the same visit were binned together and hence we were left with 67 final spectra from Barycentric Julian Dates 2458872.01645143 to 2459682.77599452. Using the SERVAL (SpEctrum Radial Velocity AnaLyzer) modified for HPF (the whole source code is present at https://github.com/gummiks/hpfserval_lhs3154), 67 Radial velocities along with their errors. No methodological changes were made in this part.

The SERVAL algorithm uses template matching instead of matching the spectra with a theoretical line model. In simpler terms, SERVAL starts off by choosing the highest Signal to Noise ratio spectra as a template for radial velocity calculation. It then iteratively estimate the radial velocities of the spectra, by slowly changing the reference template (Zechmeister et al., 2018). This template fitting method has been shown to more accurately predict M-dwarf radial velocities compared to other methods, and was thus used by the original authors (Anglada-Escudé and Butler, 2012).

Stefánsson et al., 2023 published their calculated Radial Velocities with their work. When we reproduced the velocities on our end, we obtain the exact same results except on 2458918.87300853 BJD. Their reported value is -19.73 ± 28.05 m s^{-1}, whereas our value is -36.69 ± 23.21 m s^{-1}. The reason for this discrepancy is unknown, as we did not change their source code at all while calculating the radial velocities. This discrepancy's implications are explored in Section 3 later.

2.2 Best fit curve and Keplerian orbit measurement

Stefánsson et al., 2023 mention they use the `JULIET` library in `python` to measure the orbital parameters. However they did not provide the source code and thus, we wrote it using the library's publicly available documentation at https://github.com/nespinoza/juliet.

`JULIET` uses Bayesian statistics to predict orbital parameters and create a best fit of the radial velocity measurements using another package called `radvel` (Fulton et al., 2018). In this method, we input our initial guess (Prior) of the distribution of all elements being modeled in the system, and then the

algorithm tries to create a best fit starting from the initial guess and outputs the distribution of the elements (Posteriors). The sampling of points from the Prior distribution was done using the `Dynesty` package inside `JULIET` (Speagle, 2020). `Dynesty` requires input of how many points will explore the hyperparameter space to find the best fit. Stefánsson et al., 2023 does not state their values, and thus we used 10000 points. `Dynesty`'s documentation states that around 300 points will provide a good enough fit while being extremely fast. We used 10000 to ensure the highest possible accuracy, even though it took a lot more computational resources. For the best fit of the orbit, a total of 7 elements were modeled.

1. Period (P): The time it takes for the exoplanet to complete one revolution around the host star, or vive versa.
2. Time of conjunction (t_0): Time at which the planet is closest to us.
3. Eccentricity (e): How circular or elliptical is the orbit.
4. Argument of Periastron (ω): The angle from the Ascending Node to the perigee (the point where the exoplanet is closest to the host star), in the plane of the orbit. However for exoplanets, it is difficult to define the ascending node and thus, it is arbitrarily chosen as the point at which the planet crosses the sky plane. This means $\omega = 90°$ corresponds to the periastron of the orbit lying in the line of sight.
5. Semi-amplitude of Radial Velocity (K): Half of the total amplitude (Maximum radial velocity to the minimum radial velocity) of the radial velocity curve.
6. Systematic Velocity (μ): The relative velocity induced on the observed system due to motion of the Earth.
7. Random Velocity (γ): Random velocity errors in the system.

The first 5 elements form the Keplerian orbit, while the last two are measurement errors that affects our observation. Do note that we are treating this as a two-body system moving about a common Barycenter, and the output of `JULIET` will be the planetary parameters and NOT the stellar parameters.

3 Results and Discussion

3.1 Orbital Period estimation and Priors

In order to best fit, we must first decide on our Priors. The prior for orbital period of the system can be estimated by observing the calculated radial velocities. Figure 2 shows the Lomb-Scargle periodogram of the observed radial velocities plotted using the `astropy` library in `Python`. A Lomb-Scargle periodogram is a visual representation of period signatures in a timeseries data. The y-axis represent the strength

of the periodic signal (VanderPlas, 2018). In our case, we observe a peak at 3.72 days, suggesting that the radial velocities could potentially have a periodicity of about 3.72 days. We also note that there are other prominent peaks in the datset, however they do not represent the true periodicity of the system and are merely aliasing. Given that we can only collect data at night, there is an inherent periodicity in the dataset of roughly 1 day. Suppose the actual frequency of the system is f_0 day^{-1}, and thus, we can expect to see another periodic signal at $(f_0 + 1)$ day^{-1}. Thus,

$$P_{1 \text{ day alias}} = \frac{1}{f_{1\text{-day alias}}} = \frac{1}{1 + \frac{1}{3.27}} \approx 0.79 \text{ days} \tag{1}$$

This signal is marked by the red dashed line. The other alias peaks are formed due to subfrequencies of this signal.

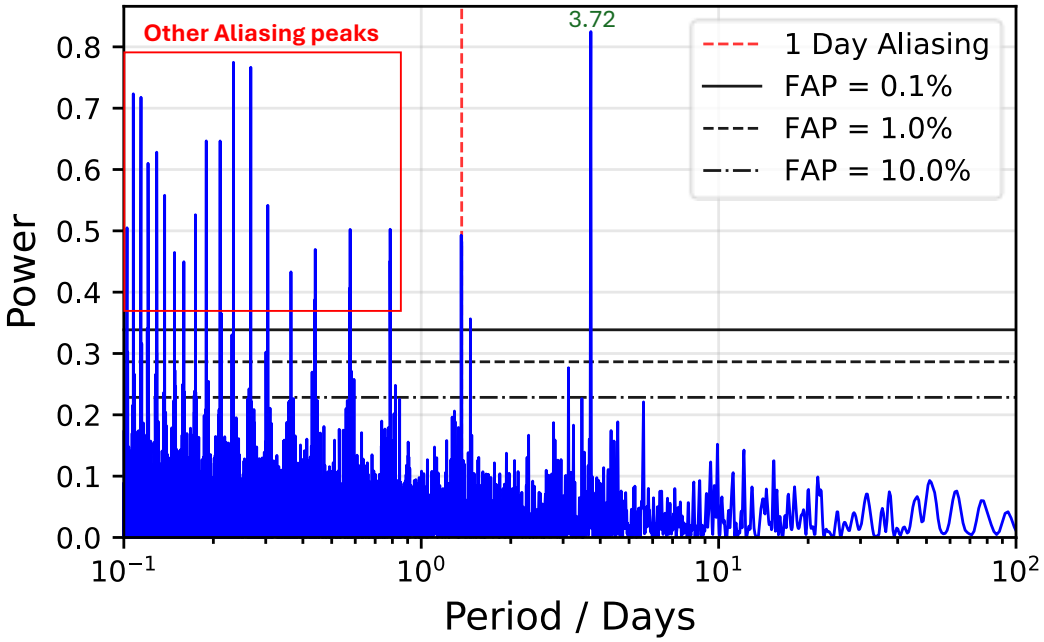

Figure 2: Lomb-Scargle Periodogram for LHS3154. We notice a very high frequency peak at 3.72 days suggesting the orbital period is close to that value. Given we could only measure at night, there is an inherent periodicity in the measurements which results in aliasing peaks. FAP stands for False Alarm Probability and it is the probability that if there is no periodic signal in the data, we will observe a peak this high.

FAP refers to False Alarm Probability which is a measure of if we assume this signal does not contain any periodic signal, we expect to see a peak this high. Given that our main peak is much higher than FAP, it further strengths this is a true signal of the system. This figure is similar to Stefánsson et al., 2023's Figure 1D.

With 3.72 days as our initial guess of the period, we input the priors as shown in Table 1 (this is the same as Stefánsson et al., 2023). $\mathcal{U}$ refers to a uniform distribution, meaning all values within the distribution has an equal chance of being selected. This is used as we do not know have any initial guess

of possible distribution. Only the time of conjunction had a narrow guess region because we could observe the radial velocity change its direction. $\mathcal{J}$ refers to a loguniform distribution meaning higher values have lower probability. This is used to model the noise as extremely high noise is unlikely in the system.

Parameter	**Prior**
P / days	$\mathcal{U}$(3,4)
$t_0 - 2458800$ / BJD	$\mathcal{U}$(72.010796685,76.010796685)
e	$\mathcal{U}$(0,0.9)
ω / °	$\mathcal{U}$(0,360)
K / ms^{-1}	$\mathcal{U}$(0,100)
μ / ms^{-1}	$\mathcal{U}$(-100,100)
γ / ms^{-1}	$\mathcal{J}$(0.1,200)

Table 1: Priors used in this reproduction and also by Stefánsson et al., 2023

3.2 Best fit parameters and Radial velocity curves

After running our `JULIET` code, the best-fit values obtained are presented in Table 2. The upper and lower bound form the 68% interval of all the values. The most important observation is that our ω differs significantly from the original work. This could be due to the difference in Radial velocity mentioned before, or simply a statistical artifact in our work due to lower computational power.

Parameter	**Our Posterior**	**Original Work's Posterior**
P / days	$3.71792^{+0.00072}_{-0.00074}$	$3.71778^{+0.00080}_{-0.00081}$
$t_0 - 2458800$ / BJD	$74.24^{+0.12}_{-0.13}$	$74.26^{+0.14}_{-0.14}$
e	$0.074^{+0.056}_{-0.052}$	$0.076^{+0.057}_{-0.047}$
ω / °	73^{+101}_{-44}	82^{+102}_{-47}
K / ms^{-1}	$23.5^{+1.2}_{-1.4}$	$23.4^{+1.5}_{-1.4}$
μ / ms^{-1}	$-2.3^{+1.0}_{-0.90}$	$-2.2^{+1.1}_{-1.1}$
γ / ms^{-1}	$1.39^{+1.9}_{-1.3}$	$1.17^{+2.2}_{-0.91}$

Table 2: The posteriors obtained in this reproduction and the posteriors obtained in the original work. We notice while everything is very similar, ω seems to differ quite a lot from the original.

Using the `radvel` package in `JULIET`, the radial velocity curve is plotted. Figure 3 shows the best fit curve along with the residuals. The Root Mean Square Error of this fit is 10.1041 ms^{-1}, suggesting it is a good fit. We do note that this best fit is not exactly the same as Stefánsson et al., 2023 Figure 1A and 1B, but that could simply be due to difference in best fit priors.

Using the best fit values, we can create the phase folded curve of radial velocity as the orbit is

periodic. At the time of conjunction, the radial velocity of the host star will be 0. Using our best-fit time of conjunction and period, we can assign a phase at each point of the orbit such that 0 is conjunction, -0.5 and 0.5 are opposition.

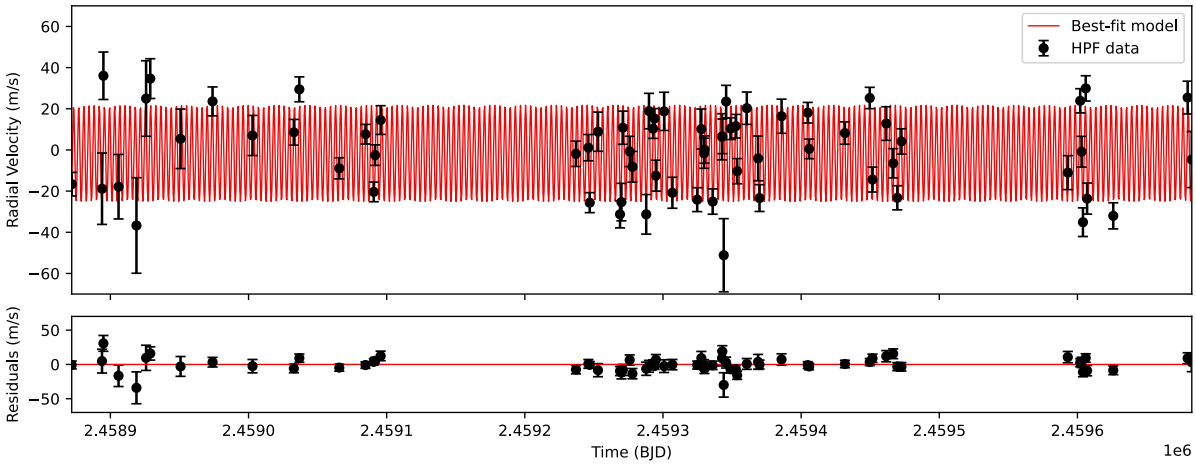

Figure 3: Best fit radial velocity curve along with the residuals. We observe the final curve is slightly different from Stefánsson et al., 2023, however the Root Mean Square Error is still low at 10.1041 ms^{-1}. The error bar represent the standard deviation errors.

Figure 4 is inverted compared to Stefánsson et al., 2023 Figure 1D and 1E, but it does not matter because its simply a choice of sign convention. While creating the phase-folded curve, we also subtracted the median value of μ as shown in Table 2. This was done to remove all effects of Earth's relative motion both from the data points and the best fit curve. The curve appears sinusoidal, which suggests that the orbit should be circular. This corroborates with the close to 0 eccentricity value obtained in our best fit.

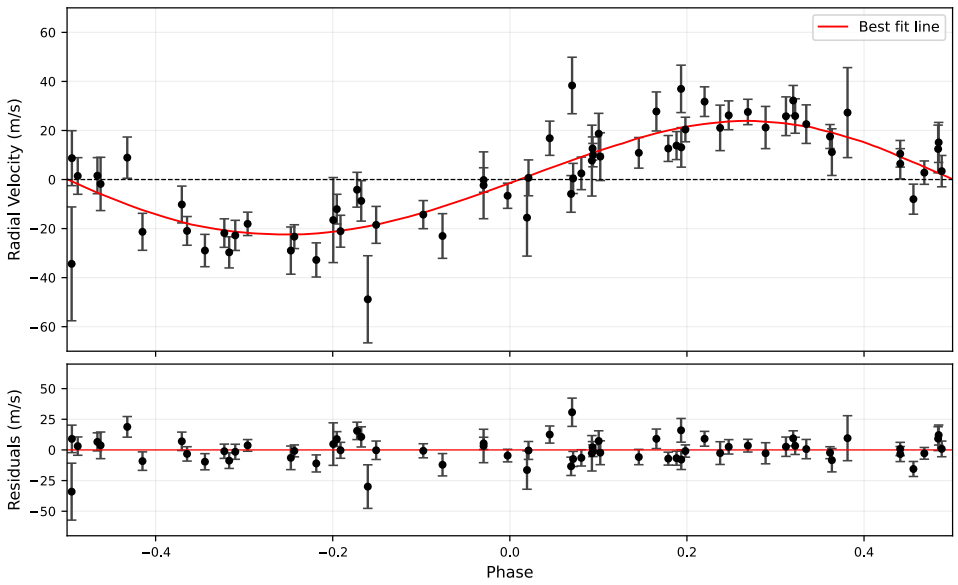

Figure 4: Best fit radial velocity curve along with the residuals in a phase-folded x-axis. We observe the final curve is inverted compared to Stefánsson et al., 2023, however that is simply due to sign convention choice. The sinusoidal shape of the curve suggests an almost circular orbit, which corresponds with our close to 0 eccentricity value. The error bar represent the standard deviation errors.

3.3 Derivation of other orbital parameters

Using the best fit values in Table 2, we can calculate the other parameters.

3.3.1 Semi-major axis of LHS3154b

Using Kepler's third Law, we can estimate the semi major axis of LHS3154b as we can assume the mass of LHS3154 is much larger than LHS3154b,

$$a = \left(\frac{G(m_1 + m_2)}{4\pi^2} P^2\right)^{\frac{1}{3}} \tag{2}$$

$$\approx \left(\frac{Gm_1}{4\pi^2} P^2\right)^{\frac{1}{3}} \tag{3}$$

Stefánsson et al., 2023 estimate the mass of the star to be 0.1118 ± 0.0027 $M_\odot$. Using this value along with the period obtained in Table 2,

$$a \approx 0.0226238^{+0.0000029}_{-0.0000030} \text{ AU} \tag{4}$$

This value is close to 0.02262 ± 0.00018 AU which was calculated by Stefánsson et al., 2023.

3.3.2 Time of periastron

The time of periastron, T_p is defined as the time at which the planet is closest to its star (at its perigee). We have defined the ascending node as 90° away from the line of sight, and thus if we assume almost circular orbit,

$$f_{\text{conj}} = 90^\circ - \omega \tag{5}$$

where f_{conj} is the true anomaly of the orbit at conjunction. From geometry, we know the relationship between the true anomaly and the eccentric anomaly is,

$$\tan\left(\frac{f}{2}\right) = \sqrt{\frac{1+e}{1-e}} \tan\left(\frac{E}{2}\right) \Rightarrow E_{\text{conc}} = 2 \arctan\left[\sqrt{\frac{1-e}{1+e}} \tan\left(\frac{f_{\text{conj}}}{2}\right)\right] \tag{6}$$

The relation between eccentric anomaly and mean anomaly is given by Kepler's equation,

$$M = E - e \sin E \tag{7}$$

and by definition,

$$M_t = \frac{2\pi}{P}(t - T_{\text{peri}}) \tag{8}$$

Combining equation 7 with 8 at conjunction gives us,

$$T_{\text{peri}} = T_{\text{conj}} - \frac{P}{2\pi}\left(E_{\text{conj}} - e\sin E_{\text{conj}}\right) \tag{9}$$

Thus, using values obtained from Table 2, we obtain,

$$T_{\text{peri}} - 2458800 \approx 73.91^{+0.72}_{-0.49}\ \text{BJD} \tag{10}$$

which is close to Stefánsson et al., 2023's calculation of $74.02^{+0.67}_{-0.57}$ BJD.

3.3.3 Minimum mass of LHS3154b

Consider an elliptical orbit, with true anomaly (angle from the periastron to the planet measured towards the descending node) θ, Arguemnt of Periastron ω, inclination i, and r be the distance between focii and the orbiting body. ω and i are constant with respect to time. We can write the line of sight velocity, or the radial velocity of the body as,

$$v_r = \frac{d}{dt}[r\sin(\theta+\omega)\sin i] \tag{11}$$

$$= \sin i\left[\dot{r}\sin(\theta+\omega) + r\dot{\theta}\cos(\theta+\omega)\right] \tag{12}$$

As the orbit is elliptical,

$$r = \frac{a(1-e^2)}{1+e\cos\theta} \tag{13}$$

$$\Rightarrow \dot{r} = a(1-e^2)(-1)(1+e\cos\theta)^{-2}(-e\sin\theta)\dot{\theta} \tag{14}$$

$$= \frac{ae\sin\theta(1-e^2)\dot{\theta}}{(1+e\cos\theta)^2} \tag{15}$$

$$= r\frac{e\dot{\theta}\sin\theta}{1+e\cos\theta} \tag{16}$$

Using Kepler's second law with the area of ellipse $A = \pi a^2\sqrt{1-e^2}$, and integrating the left side over 1 period,

$$\frac{dA}{dt} = \frac{1}{2}r^2\dot{\theta} \tag{17}$$

$$\Rightarrow \frac{A}{P} = \frac{1}{2}r^2\dot{\theta} \tag{18}$$

$$\Rightarrow r\dot{\theta} = \frac{2\pi a^2\sqrt{1-e^2}}{rP} \tag{19}$$

Substitution equation 14 in equation **??** gives us,

$$r\dot{\theta} = \frac{2\pi a(1 + e\cos\theta)}{P\sqrt{1-e^2}} \tag{20}$$

And, substituting equation 21 in 16 gives us,

$$\dot{r} = \frac{2\pi ae\sin\theta}{P\sqrt{1-e^2}} \tag{21}$$

Finally, substituting equation 19 and 21 in equation 12, and applying trigonometric identities gives us,

$$v_r = \frac{2\pi a\sin i}{P\sqrt{1-e^2}}[\cos(\theta+\omega) + e\cos(\omega)] \tag{22}$$

We now have a expression for the semi-amplitude of radial velocity,

$$K = \frac{2\pi a\sin i}{P\sqrt{1-e^2}} \tag{23}$$

Substituting equation 3 in equation 23, we obtain

$$K \approx \left(\frac{2\pi G}{Pm_1^2}\right)^{1/3} \frac{m_2\sin i}{\sqrt{1-e^2}} \tag{24}$$

$$m_2\sin i \approx K\sqrt{1-e^2}\left(\frac{Pm_1^2}{2\pi G}\right)^{\frac{1}{3}} \tag{25}$$

Using the mass of the planet estimated by Stefánsson et al., 2023 and the values we obtain in Table 2,

$$m\sin i \approx 13.21^{+0.68}_{-0.79}\ \mathrm{M}_E \tag{26}$$

This value is consistent with Stefánsson et al., 2023's calculated value of $13.15^{+0.84}_{-0.82}$ M_E. This gives a planet to star mass ratio of about 0.0032, which Stefánsson et al., 2023 has shown to be an outlier when compared to other planets around M-dwarfs in their Figure 2. We do not reproduce the figure here as it does not add to our analysis of the paper.

3.4 Why is this exoplanet special?

From our calculations and predictions, the semi major axis of the planet is very small, the orbit is almost circular, and the mass of the planet is comparable to the mass of Neptune (≈ 17.15 M_E).

As per our current theories, there are two mechanisms through which planets can form around a M-dwarf star. The first mechanism is **core accretion**. In this mechanism, we assume that there was a proto planetary disk around the star. In these disks, planetesimals would form. These are small kilometer sized

bodies which, due to their relatively larger mass compared to other grains in the proto planetary disk stars to accrete grains and increase in size. These planetesimals can grow and form planets. However, simulations have shown that around smaller mass host stars such as M-dwarfs, the planets formed are either low mass with short semi major axis, or high mass with large semi major axis (Liu et al., 2020). Both scenarios are the exact opposite of LHS3154b's existence. Stefánsson et al., 2023 Figure 3 shows the core accretion simulation adopted from Liu et al., 2020, however it is not reproduced here as it does not add to our analysis of the paper.

The other possible mechanism is **gravitational instability**. This method says that instead of formation of planetesimals, if the proto planetary disk is massive enough, its self-gravity could cause it to collapse on itself directly forming massive protoplanets and thus massive planets. However, work has shown that this theory prefers massive planet formation at large semi-major axis (Boss, 2011). This theory, again, predicts contrary to the exitence of LHS3154b.

The inability of our current models to explain LHS3154b's formation either makes it an outlier, or points at gaps in our current models. More discoveries of exoplanets around M-dwarf stars could improve our understanding.

4 Conclusion

In this analysis, we reproduced all the planetary parameters found by Stefánsson et al., 2023 in their work and their Figures 1 and 2. We calculated the time of conjunction, argument of periastron, semi amplitude of radial velocity, eccentricity of the orbit, and the orbital period of LHS3154b through radial velocity curve fitting by `JULIET`. Then, we derived the time of periastron, semi-major axis, and the minimum mass of the planet through orbital mechanics. Given that our calculated value of one of the Radial velocity differs from their published dataset and the unknown precision of the `Dynesty` run, our final values are slightly different. However they still lie within error ranges. The minimum mass of the planet is around 13.2 M_E with a semi-major axis of 0.0226 AU, suggesting that it is a massive planet in very close proximity to a small mass M-dwarf star. However, neither core accretion mechanism nor the gravitational instability mechanism of planet formation can explain such mass and orbit. This makes LHS3154b special and a challenge to our current understanding of planet formation.

5 References

Anglada-Escudé, G., & Butler, R. P. (2012). THE HARPS-TERRA PROJECT. i. DESCRIPTION OF THE ALGORITHMS, PERFORMANCE, AND NEW MEASUREMENTS ON a FEW REMARKABLE STARS OBSERVED BY HARPS. *The Astrophysical Journal Supplement Series*, *200*(2), 15. https://doi.org/10.1088/0067-0049/200/2/15

Boss, A. P. (2011). FORMATION OF GIANT PLANETS BY DISK INSTABILITY ON WIDE ORBITS AROUND PROTOSTARS WITH VARIED MASSES. *The Astrophysical Journal*, *731*(1), 74. https://doi.org/10.1088/0004-637X/731/1/74

Fulton, B. J., Petigura, E. A., Blunt, S., & Sinukoff, E. (2018). RadVel: The Radial Velocity Modeling Toolkit., *130*(4), 044504. https://doi.org/10.1088/1538-3873/aaaaa8

Gaia Collaboration, Arenou, F., Babusiaux, C., Barstow, M. A., Faigler, S., Jorissen, A., Kervella, P., Mazeh, T., Mowlavi, N., Panuzzo, P., Sahlmann, J., Shahaf, S., Sozzetti, A., Bauchet, N., Damerdji, Y., Gavras, P., Giacobbe, P., Gosset, E., Halbwachs, J.-L., ... Zucker, S. (2023). *Gaia* data release 3: Stellar multiplicity, a teaser for the hidden treasure. *Astronomy & Astrophysics*, *674*, A34. https://doi.org/10.1051/0004-6361/202243782

Liu, B., Lambrechts, M., Johansen, A., Pascucci, I., & Henning, T. (2020). Pebble-driven planet formation around very low-mass stars and brown dwarfs [Publisher: arXiv Version Number: 1]. https://doi.org/10.48550/ARXIV.2004.07239

Speagle, J. S. (2020). DYNESTY: a dynamic nested sampling package for estimating Bayesian posteriors and evidences., *493*(3), 3132–3158. https://doi.org/10.1093/mnras/staa278

Stefánsson, G., Mahadevan, S., Miguel, Y., Robertson, P., Delamer, M., Kanodia, S., Cañas, C. I., Winn, J. N., Ninan, J. P., Terrien, R. C., Holcomb, R., Ford, E. B., Zawadzki, B., Bowler, B. P., Bender, C. F., Cochran, W. D., Diddams, S., Endl, M., Fredrick, C., ... Zeimann, G. (2023). A neptune-mass exoplanet in close orbit around a very low-mass star challenges formation models. *Science*, *382*(6674), 1031–1035. https://doi.org/10.1126/science.abo0233

VanderPlas, J. T. (2018). Understanding the lomb–scargle periodogram. *The Astrophysical Journal Supplement Series*, *236*(1), 16. https://doi.org/10.3847/1538-4365/aab766

Zechmeister, M., Reiners, A., Amado, P. J., Azzaro, M., Bauer, F. F., Béjar, V. J. S., Caballero, J. A., Guenther, E. W., Hagen, H.-J., Jeffers, S. V., Kaminski, A., Kürster, M., Launhardt, R., Montes, D., Morales, J. C., Quirrenbach, A., Reffert, S., Ribas, I., Seifert, W., ... Wolthoff, V. (2018). Spectrum radial velocity analyser (SERVAL): High-precision radial velocities and two alternative spectral indicators. *Astronomy & Astrophysics*, *609*, A12. https://doi.org/10.1051/0004-6361/201731483